**Polymer Degradation and Stability**
September 2021, Volume 191, Pages 109657 (11p.)
https://doi.org/10.1016/j.polymdegradstab.2021.109657
https://archimer.ifremer.fr/doc/00701/81324/



# Origin of embrittlement in Polyamide 6 induced by chemical degradations: mechanisms and governing factors

Deshoulles Quentin [1, 2], Le Gall Maelenn [1], Dreanno Catherine [2], Arhant Mael [1], Stoclet G. [3], Priour Daniel [1], Le Gac Pierre Yves [1, *]

[1] Laboratoire Comportement des Structures en Mer, Ifremer, Centre de Bretagne, 29280 Plouzané, France
[2] Laboratoire Détection Capteurs et Mesures, Ifremer, Centre de Bretagne, 29280 Plouzané, France
[3] Université de Lille, INRA, ENSCL, UMR 8207,Unité Matériaux et Transformation, F-59000, Lille, France

* Corresponding author : Pierre Yves Le Gac, email address : pierre.yves.le.gac@ifremer.fr

**Abstract :**

Polyamide 6 films were immersed in two ageing environments inducing either only oxidation or only hydrolysis of the polymer for up to two years. Ageing temperatures ranged from 80°C to 140°C. Samples were characterized periodically in terms of both chemical structure at the macromolecular scale, using SEC, DSC, SASX and WAXS, and mechanical behaviour through tensile tests. Both degradation mechanisms lead to chain scission within the polymer, an increase in crystallinity ratio, a decrease in the amorphous layer thickness and an embrittlement of the polymer. First a decrease in the strain at break is observed while the maximal stress remains unchanged. Then a drop in maximal stress is identified. Using these experimental results, both the origin of the embrittlement and the factors governing embrittlement are discussed. The decrease in strain at break is attributed for the first time in polyamide to the decrease in concentration of tie molecules determined through a theoretical approach. The loss in entanglements is associated with the drop in maximal stress. Furthermore, it is shown that the crystallinity ratio does not govern the embrittlement of polyamide. However, both the molar mass and the amorphous layer thickness are faithful indicators of this embrittlement whatever the degradation mechanism.

**Highlights**

► Decrease in strain at break during polyamide ageing is due to decrease in tie molecule concentration
► Both molar mass and amorphous layer thickness can be used to describe embrittlement in polyamide
► Crystallinity ratio cannot be used to describe embrittlement in polyamide

**Keywords** : Polyamide, Embrittlement, Hydrolysis, Oxidation Tie molecules

# 1.Introduction

Secondary microplastics are defined as small pieces of plastic (5 mm and less) originating from macroplastics fragmentation in the oceans [1]. This fragmentation is due to polymer embrittlement with time induced by chemical ageing of the material. The concern about secondary microplastic formation has raised new scientific questions that have to be answered in order to better understand the behaviour of these particles and their potential impact on the environment [2, 3]. One of these questions is how chemical ageing leads to brittle polymers and more especially what are the factors governing this embrittlement when polymers are subjected to advanced degradation.

Polyamide materials are widely used by the automotive industry [4-6], in oil and gas application, and also for wind turbine moorings [7]. Polyamide production has increased in the last 20 years to reach 5.5 million tonnes in 2015 [8] so the long-term behaviour of these polymers will become important in the future. The durability of polyamide 6 (PA6) has already been largely studied in the past and one of its main features is that this polymer absorbs a large amount of water when in contact with a humid environment, up to 10% when immersed in sea water [9]. The presence of water within the polymer leads to a plasticization of the material, i.e. a reversible increase in macromolecule mobility, that results in a large decrease in glass transition temperature ($T_g$) from 60°C (in the dry state) to -20°C (after immersion in sea water, [10, 11]). Chemical degradation can also occur in PA6, according to two main degradation processes: hydrolysis and oxidation [12-15]. These degradations mainly lead to chain scissions in the polymer that becomes brittle as degradation occurs [16, 17]. Although embrittlement in polyamide material has already been described in the past, the exact factors governing this process remain unclear.

Embrittlement in amorphous polymers has been studied for several decades. Thus, several structural parameters have been identified as potential indicators of the embrittlement. It has been found that a critical molecular mass named $M'_c$ can be defined [18,19]. When the average number molecular mass ($M_n$) of the polymer is below $M'_c$ the polymer exhibits a brittle behaviour. It has been shown that the $M'_c$ value is equal to 5 $M_e$ where $M_e$ is the entanglement molar mass [20]. When considering semi crystalline polymers, it becomes much more complex because the crystalline part largely affects the mechanical behaviour of the material. Most of the existing work has focussed on semi crystalline polymers with an amorphous phase in the rubbery state at room temperature such as Polyethylene (PE) or Polypropylene (PP) [21,22]. Usually, embrittlement of the polymer is related with more or less success to the crystallinity ratio [23,24] or the molecular weight [25]. As for amorphous polymers, a critical molecular mass has been observed in the literature [19,26]. However, the value of $M'_c$ for semi-cristalline polymers is much higher ($M'_c$ = 50 $M_e$), which highlights the role of the crystalline structure. Another parameter that seems to be particularly relevant to describe embrittlement in semi crystalline polymers is the thickness of the amorphous layer between two crystalline lamellae (considering a stacked model), named $l_a$. Regarding PE, the most studied polymer in the literature, it has been shown that $L_a$ can be used to describe embrittlement of this polymer [27,28]. When $L_a$ is above 6 nm, the stress can be transferred to crystallites by the amorphous phase, slipping of crystals can occur and a plastic deformation exists; in this case, the sample exhibits a ductile behaviour. On the contrary when $l_a$ is lower than 6 nm PE is brittle. For semi crystalline polymers with an amorphous region in the glassy state, there is much less data available in the literature. In a recent paper dealing with thermal oxidation of polyamide 11, it has been suggested that the embrittlement process is not affected by the state of the amorphous phase and both $M_n$ and $L_a$ can be used to describe the embrittlement [16]. Moreover, authors found that the critical value for $L_a$ is about 6 nm and suggest that this value can be universal for all semi crystalline polymers.

To study polymer embrittlement, the morphology of the polymer is usually changed by using thermal treatments [28], modifying conditions such as testing temperature [29], or modifying the polymer chemistry. In this study another approach, i.e a chemical ageing process, is used. In order to understand factors governing the embrittlement, a polyamide 6 film has been subjected to different ageing conditions in order to modify its structure. Two ageing environments are considered here, water and air, with several ageing temperatures and durations. By using this experimental design, samples with various properties were obtained allowing the origin of the embrittlement to be investigated in detail. Overall, more than 50 conditions were studied considering both mechanical behaviour and the polymer properties such as molecular weight, crystallinity ratio and nature of crystalline phases. First, all the results will be presented and then the factors governing embrittlement in polyamide will be discussed.

# 2. Material and methods

## 2.1. Material

Two types of samples were used in this study; both are polyamide 6 films without stabilizers. For ageing in water, samples were 250 µm thick. The thickness was chosen to obtain a homogenous degradation through thickness during hydrolysis and also to allow mechanical characterization even when the polymer is brittle. For thermal oxidation, it was necessary to decrease the sample thickness down to 75 µm to avoid heterogeneous degradation on account of the Diffusion Limited Oxidation (DLO) phenomenon [30, 31]. However, the mechanical characterization of such thin samples is quite difficult. The main characteristics of the unaged samples are presented in Table 1. The films were produced by extrusion. The tensile samples were systematically cut in the direction of the extrusion.

Table 1 – Main properties of the two polyamides used in this study, tested in dry conditions

| **Property in dry state** | **PA6 250 µm** | **PA6 75 µm** |
|---|---|---|
| $T_g$ (°C) | 52 ± 1 | 57 ± 2 |
| Melting temperature (°C) | 220 ± 1 | 221 ± 1 |
| Degree of crystallization (%) | 20 ± 1 | 26 ± 1 |
| Strain at break (%) | 370 ± 12 | 30 ± 8 |
| Yield Stress (MPa) | 70 ± 1 | 68 ± 1 |
| Mn (kg/mol) | 53 ± 1 | 36 ± 1 |

## 2.2. Ageing

Two types of ageing experiment are considered in this study. One is performed in ovens where only thermal oxidation occurs, the other one is carried out in water without oxygen where only hydrolysis occurs.

Oxidative degradation was carried out by placing samples in ovens (type UN55, Memmert) at temperatures ranging from 100°C to 140°C ± 1°C. A continuous convection of air was applied in order to ensure a homogeneous temperature in the oven.

Hydrolytic degradation was performed using pressure vessel tanks filled with deionised water at temperatures ranging from 80°C to 140°C ± 1°C. Nitrogen bubbling was performed in the water prior to ageing using a nitrogen generator (Parker Dominik Hunter G2000E) for a minimum duration of 3 hours. Samples were dried at 40°C in a desiccator at a relative humidity of 0% until mass stabilization was reached prior to characterization. More details are available in [32].

## 2.3. GPC (Gas Permeation Chromatography)

GPC measurements were performed according to the method described by Laun et al. [33]. Samples were dissolved in 1,1,1,3,3,3-hexafluoroisopropan-2-ol (HFiP) and then injected in a Water 2695 chromatograph at a flow rate of 1 ml/min. A differential reactive index detector was used to perform detection and data was processed with PSS WinGPC unity v7.5 SEC software. The calibration was based on poly(methyl methacrylate) standards supplied by PSS GmbH Mainz, Germany, with molar mass ranging between 800 and 1,600,000 g $mol^{-1}$, and the calibration curve was adjusted with a 5th order polynomial.

## 2.4. DSC (Differential Scanning Calorimetry)

DSC measurements were performed using a Q200 device (TA instrument). Testing was done under a nitrogen flow (50ml/min) at a rate of 10°C/min. 3 samples were tested per condition. The crystallinity ratio was calculated using Eq. 1:

$$\chi_c = \frac{\Delta H_f}{\Delta H_f^o} * 100 \qquad \text{(Eq. 1)}$$

Where $X_c$ is the crystallinity ratio in %, $\Delta H_f$ is the measured melting enthalpy (J/g) and $\Delta H_f^o$ is the melting enthalpy of a fully crystalline PA6 and taken equal to 240 J/g [34,35].

## 2.5. X-Ray measurements

WAXS and SAXS measurements were performed on a Xeuss 2.0 apparatus (Xenocs) equipped with a micro source using a Cu Kα radiation (λ =1.54 Å) and point collimation (beam size: 300×300 µm²). The sample to detector distance, around 15 cm for WAXS and 1.5 m for SAXS, was calibrated using silver behenate as the standard. Through view 2D diffraction patterns were recorded on a Pilatus 200k detector (Dectris). Integrated intensity profiles were computed from the 2D patterns using the Foxtrot® software. The long period was computed using Equation 2:

$$L_p = \frac{2\pi}{q_{max}} \quad \text{(Eq. 2)}$$

Where $L_p$ is the long period (nm) and $q_{max}$ (nm) the maximum of the correlation peak.

The amorphous layer thickness was defined by Equation 3 from the long period $L_p$ (previously defined using Equation 2 with SAXS measurements) and the crystallinity ratio (from DSC measurements), using Equation 4:

$$l_a = L_p - l_c \text{ (Eq. 3)}$$

$$l_c = \chi_c \frac{L_p \rho_a}{\rho_c - \chi_c(\rho_c - \rho_a)} \text{ (Eq. 4)}$$

Where $l_a$ and $l_c$ are respectively the amorphous and crystalline layer thicknesses (nm), $L_p$ the long period (nm), $\chi_c$ the crystallinity ratio (%), $\rho_a$ and $\rho_c$ respectively amorphous and crystalline phase density (g/cm$^3$).

## 2.6. Tensile tests

Tensile tests were carried out under dry conditions using a 10 kN capacity tensile machine (Instron™) with a 500 N load cell and a displacement rate of 1 mm/min. Samples were dumbell shaped specimens, type 3 from ISO 37 [36] and the strain was measured using an optical extensometer (type AVE2). At least 5 samples were characterized per condition.

# 3. Results

This section is devoted to the changes occurring during both hydrolysis and thermo oxidation in terms of physico-chemical and mechanical properties.

The average number of molecular mass (Mn) is plotted as a function of ageing time when samples are immersed in water at temperatures ranging from 80°C to 140°C (Figure 1 a). A clear decrease in Mn is observed when ageing duration increases; this is the result of chain scission that occurs due to the hydrolysis of amide bonds [37–39]. Obviously when ageing temperature increases, the decrease in Mn is faster. When ageing is performed in air for temperatures ranging from 100 to 140°C, a decrease of Mn is also observed (Figure 1b) and this is associated to chain scission in the polymer that is the major process during polyamide oxidation. [40]. For all data points presented here there is no large change in the polydispersity index, that is equal to 2.5 ± 0.5.

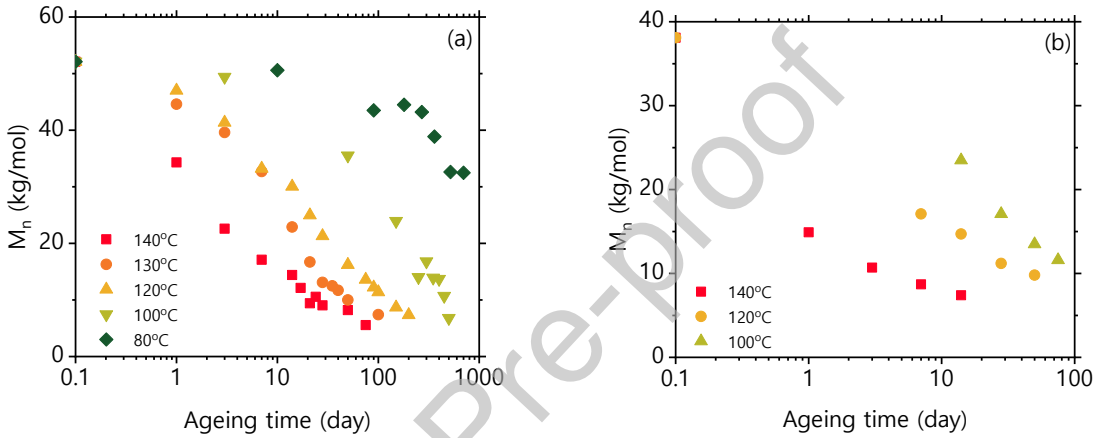


Figure 1 – Change in $M_n$ as function of ageing time when samples are immersed in water (a) and placed in air (b)

## 3.2. Crystallinity ratio

For all samples an increase in the crystallinity content in the polyamide 6 was observed (Figures 2a and 2b). It is worth noting that during ageing in water two different processes are involved. Initially a fast increase in crystallinity occurs, which then slows down withtime (from 20 to 40% in one day at 140°C in water). The first increase occurs within a few minutes when samples are immersed in hot water (i.e. 140°C) and depends largely on ageing temperature; this process will be described in more detail in the next section. The second process is related to the well-known chemi-crystallization phenomenon [41]. It is caused when chain scissions occur within the polymer, there is a change in the mobility of macromolecules that can be incorporated into the crystalline phases, which leads to an increase in crystallinity; in this case the increase in crystallinity ratio is directly proportional to chain scission concentration [16]. In order to get a better characterization of the nature of the crystalline lattice, X-Ray measurements have been performed, results are presented in the next section. In air, only chemi-crystallization occurs during ageing as already reported in previous studies [42,43].

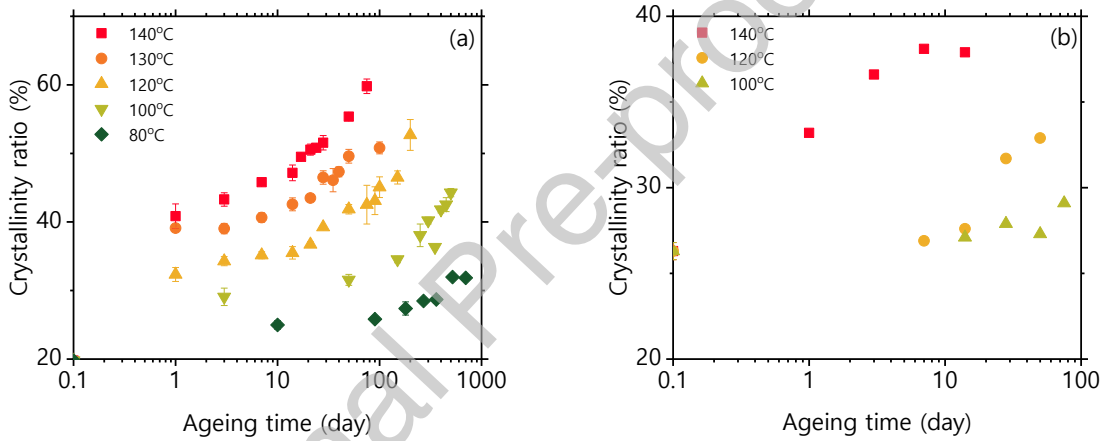


Figure 2 – Change in crystallinity ratio as function of ageing time when samples are immersed in water (a) and placed in air (b)

## 3.3. Wide Angle X-ray Scattering WAXS

The change in crystalline structure was followed by X-Ray Diffraction. Wide Angle X-Ray Scattering patterns after ageing at 120°C in water are presented in Figure 3.a. The evolution of the volume fraction of the different phases with time is shown in Figure 3b.

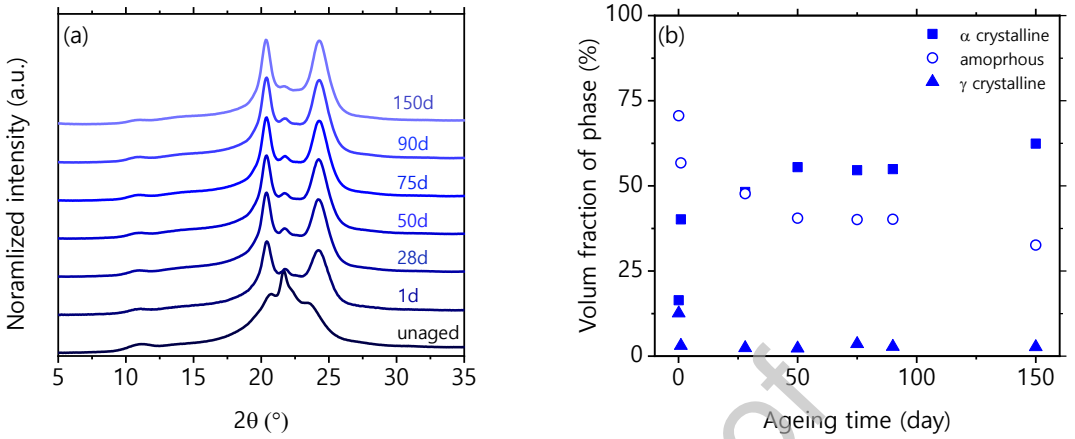


Figure 3 – Change in WAXS pattern (a) and in crystalline lattice (b) as function of ageing time in water at 120°C without oxygen

Based on the patterns shown in Figure 3.a, three different phases have to be considered here: the pseudo hexagonal γ phase (with peaks at 11°, 21.7° and 22.3°), the monoclinic α phase (with peaks at 20.4° and 24.3°) and the amorphous phase [44]. From Figure 3b we can clearly see a fast increase of the α phase content due to the transformation of the amorphous phase that is thermally less stable [45]. This transformation corresponds to the fast increase in crystallinity ratio observed by DSC in Figure 2.a. It is important to note that this transformation occurs only when water is present within the polymer and depends on temperature as shown in Figure 4. This behaviour has been explained by Gianchandani et al who suggested that in the presence of water hydrogen bonding can be partially destroyed by water molecules. This allows chain rearrangement needed to form the α phase [46]. This last point explains the fact that the crystalline lattice is not affected by temperature (up to 140°C) when samples are placed in a dry environment.

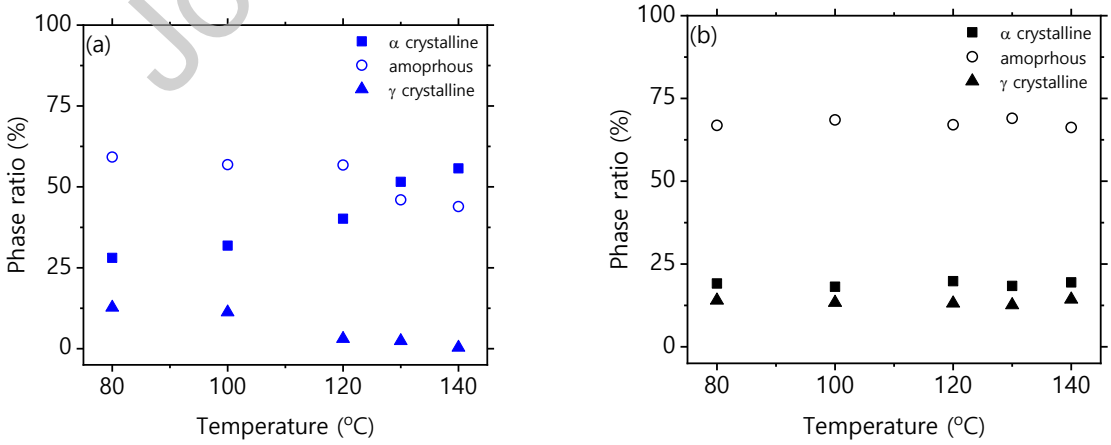


Figure 4 – Change in phase ratio after 24 hours as function of temperature in water (a) and in air (b)

For longer ageing duration (*i.e*. more than a day), a slow increase in the α phase is observed (Figure 3.b). This corresponds to the increase in crystallinity ratio and is attributed to the chemi-crystallization process as noted previously.

## 3.4. Small Angle X Ray Scattering.

Small Angle X Ray Scattering characterization was performed in order to assess the long period ($L_p$) in the polymer as a function of ageing. Integrated intensity profiles are presented in Figure 5.

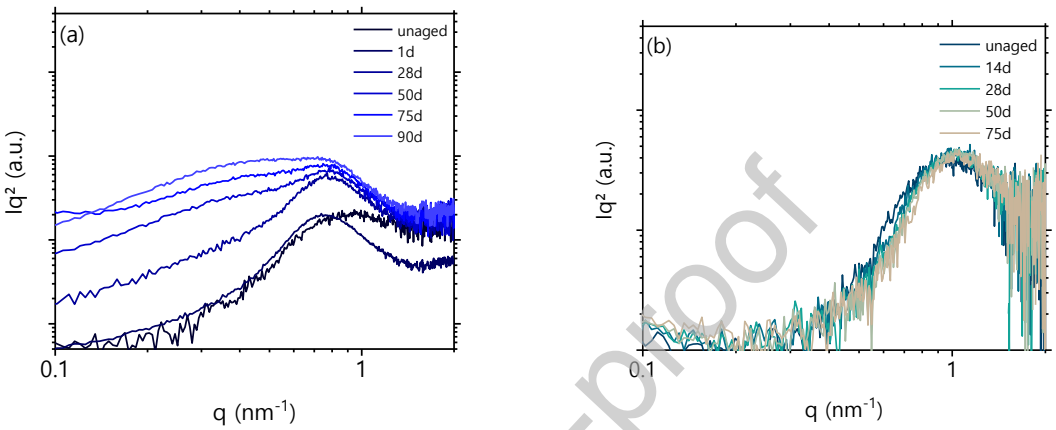


Figure 5 - SAXS integrated intensity profiles as function of ageing time at 120°C in water (a) and 100°C in air (b)

When a correlation peak is clearly observed (up to 50 days) it is possible to determine $L_p$ (Eq. 2) and therefore the thickness of the amorphous layer thanks to the crystallinity ratio assessed by DSC (Eq. 4). For longer ageing durations, it is no longer possible to distinguish a clear peak in intensity, probably due to a chaotic organization at the macromolecular scale. When ageing is performed at 100°C in air, $L_p$ can be determined for all the ageing durations considered here (Figure 5). $L_p$ is roughly constant whatever the aging duration. Using these results and the crystallinity ratio, amorphous layer thickness ($l_a$) can be estimated with Eq 4. as depicted in Figure 6.

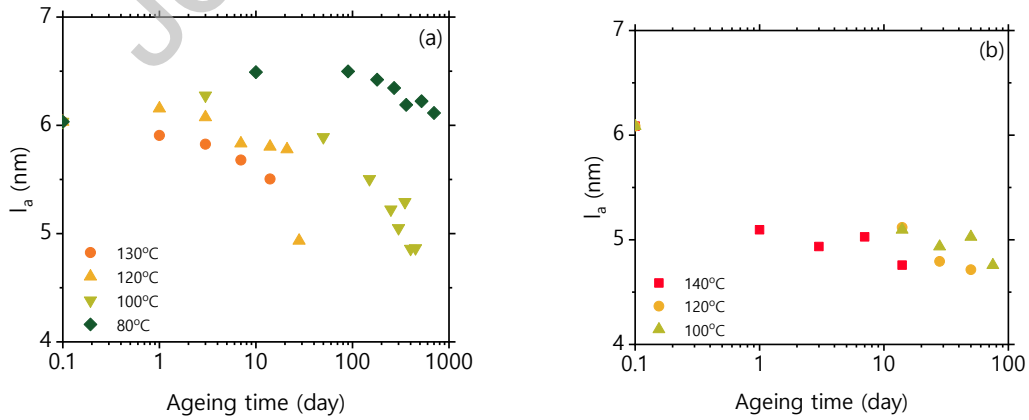


Figure 6 – Changes in the amorphous layer thickness as function of ageing time when samples are immersed in water (a) and placed in air (b)

## 3.5. Tensile Tests

The mechanical behaviour was characterized by tensile tests at a relatively low strain rate (Figure 7). The unaged material exhibited a ductile behavior, characteristic of the plastic deformation mechanism, i.e. the stress increases linearly with strain in the elastic region and then a yield in stress can be observed. Regarding PA6, it seems that the exact structural processes involved during plastic deformation are still not well understood , but at least we know that both crystal shear and cavitation in the amorphous region are involved [47]. When chain scissions take place in the polymer, a decrease in elongation at break occurs without large changes in yield stress or modulus (from 1 to 28 days, Figure 8). For longer durations, no plastic deformation occurs, the polymer exhibits a brittle behaviour and a decrease in maximal stress is observed. This decrease in maximal stress and strain at break in time was observed for all the ageing conditions considered here, as shown in Figure 8.

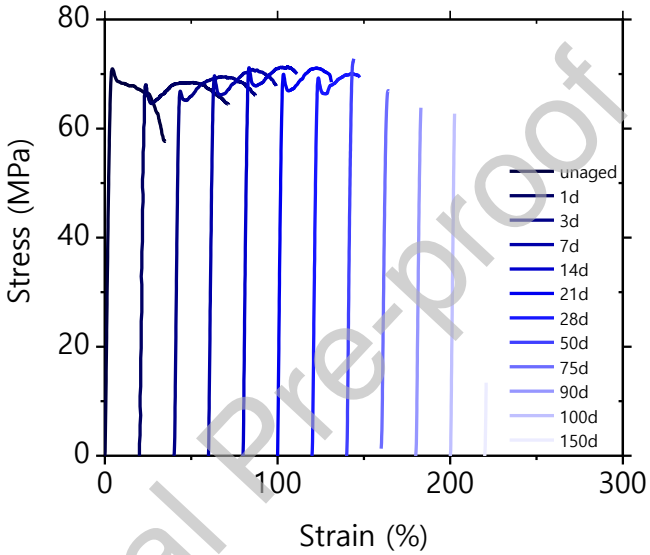


Figure 7 - Stress/strain curve as function of ageing time at 120°C in water without oxygen (tensile curves have been shifted for sake of clarity)

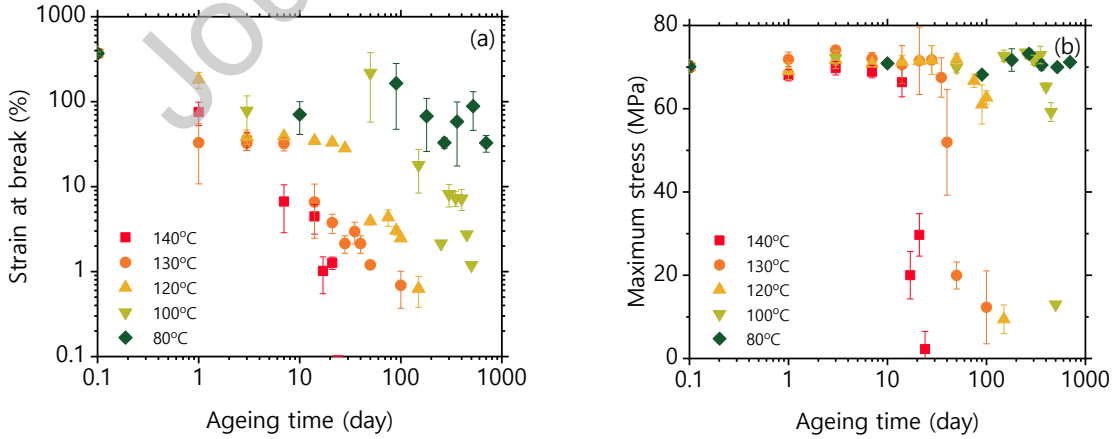

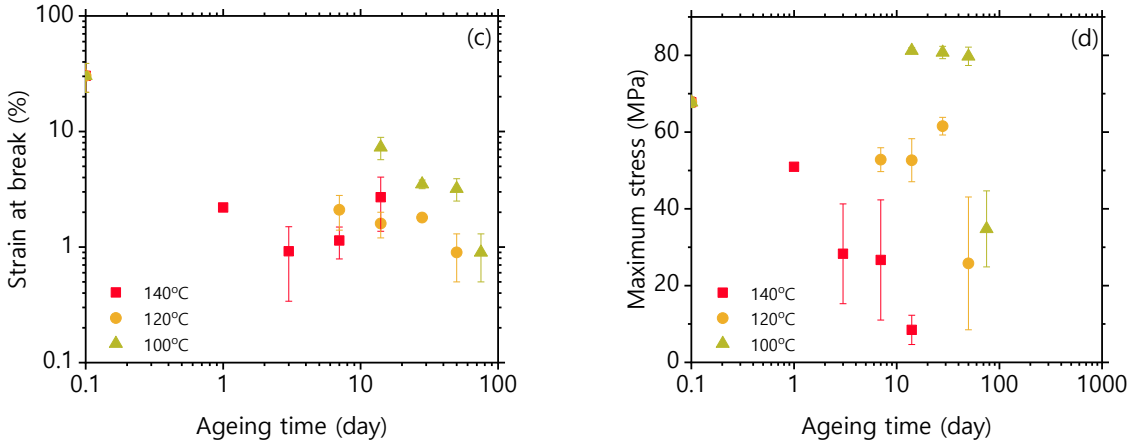


Figure 8 – Change in elongation at break and maximal stress as function of ageing time when samples are immersed in water (a, b) and placed in air (c, d)

Based on the data presented inthis section, the factors governing embrittlement in polyamide will be discussed below.

# 4. Discussion

This section aims to understand the factors governing the change from a ductile to a brittle behaviour in PA6 induced by ageing. Three different structural parameters will be considered here, the crystallinity ratio, the molecular mass and the thickness of the amorphous layer. These parameters will be discussed with regards to both maximal stress and strain at break because these two parameters are usually used for life time prediction in polymers [48–50].

## 4.1. Factors governing embrittlement

### 4.1.1. Crystallinity ratio

During both hydrolysis and oxidation processes, the crystallinity ratio increases in PA6. In order to understand the role of crystallinity ratio on embrittlement, the strain at break and maximal stress are plotted as a function of crystallinity ratio in Figure 9. No clear relationship is apparent between the crystallinity ratio and the elongation at break, indicating that it is not possible to directly link the elongation at break with the amount of crystallinity in PA6 (Figure 9a). In Figure 9.b, during the hydrolysis process, it appears that for a crystallinity ratio below 45% the maximal stress remains constant, meaning that the polymer exhibits a ductile behaviour. For a crystallinity ratio above 45% a drop in maximal stress is observed due to embrittlement of the polymer. Thus, based on results obtained only during hydrolysis it appears that a critical value of crystallinity ratio can be defined. However, when considering results from thermal oxidation, a drop in maximal stress is observed even for crystallinity ratios below 45%. This indicates that this criterion cannot be considered as a generic way to describe embrittlement in polyamide.

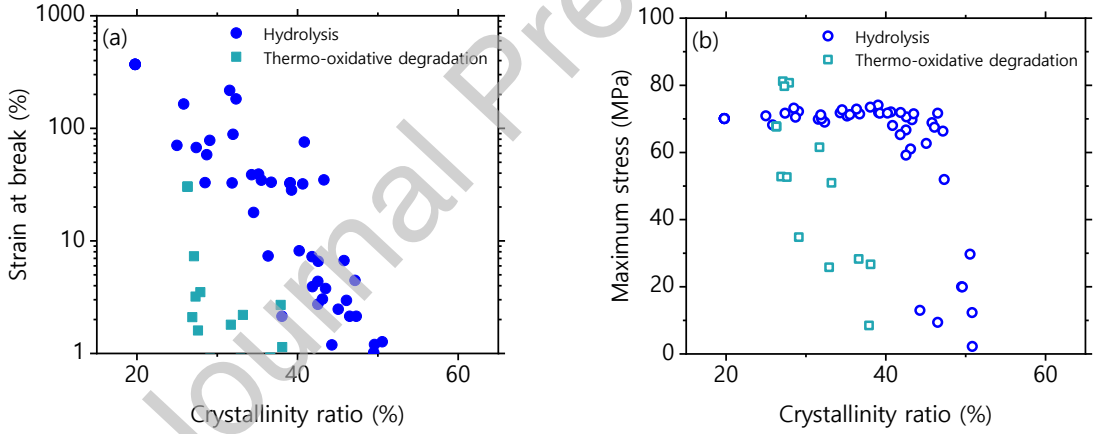


Figure 9 – Strain at break (a) and Maximal stress (b) as function of crystalinity ratio for all ageing conditions considered in this study

To conclude on crystallinity ratio, it appears that it is not possible to define a general relationship between the mechanical behaviour of polyamide and the crystallinity ratio. This means that embrittlement during ageing is not directly governed by the change in amount of crystallites

### 4.1.2. Molar mass

The molecular mass is also used to describe the transition between a ductile and a brittle behaviour for many polymers undergoing degradation processes such as hydrolysis [51,52], radiolysis [53,54] or oxidation [55,56]. Here, both strain at break and maximal stress measured during tensile characterization are plotted as a function of the $M_n$ value (Figure 10) The decrease in strain at break can be related to the molar mass using an empirical relationship as shown in Figure 10.a. Figure 10.b shows a plot of the maximal stress as a function of $M_n$ for results obtained in the present work (for both hydrolysis and oxidation) together with published data. Two types of behaviour can be highlighted: the polymer is ductile with a constant maximal stress whereas when $M_n$ > 15 kg/mol; the polymer becomes brittle and the maximal stress decreases sharply with the decrease in Mn when $M_n$<15 kg/mol A critical molar mass value can be defined here equal to 15 kg/mol. To our knowledge, this is the first time that M'c has been determined for PA6.

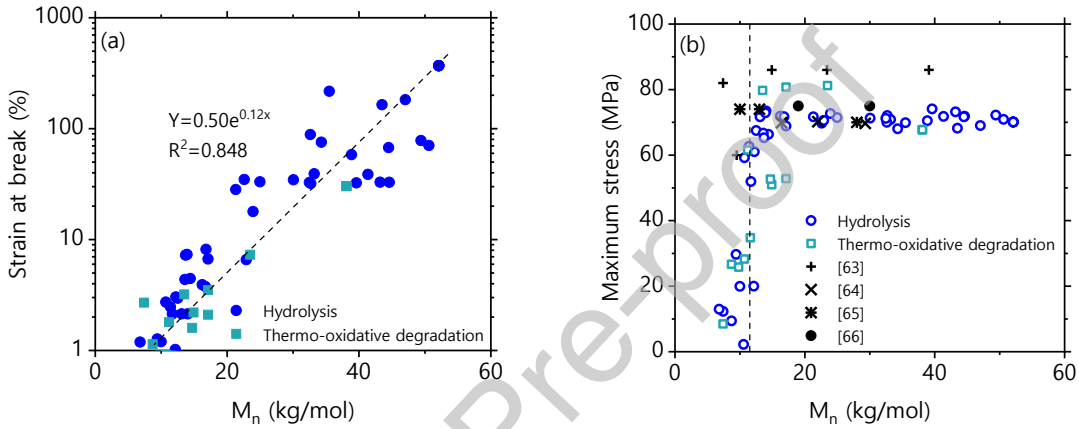


Figure 10 – Strain at break (a) and Maximum stress (b) as a function of Mn for all ageing conditions considered in this study together with data available in the literature

### 4.1.3. Thickness of the amorphous layer

The thickness of the amorphous layer is also considered in the literature to describe embrittlement in semi crystalline polymers [16,27,57]. It has been proposed by Robbelin-Souffaché and Rault considering PE that $l_a$ is directly related to the molar mass - [58] according to Equation 5.

$$la = la_0 + \alpha * M_w^{\frac{1}{2}} \quad \text{(Eq. 5)}$$

Where $l_a$ is the amorphous layer thickness in nm, $la_0$ a constant that depends on the polymer in nm, α a material constant in $(mol/kg)^{1/2}$ and $M_w$ the molar mass in weight in kg/mol. Figure 11 ~~now~~ shows the amorphous layer thickness as a function of the square root of molar mass by weight.

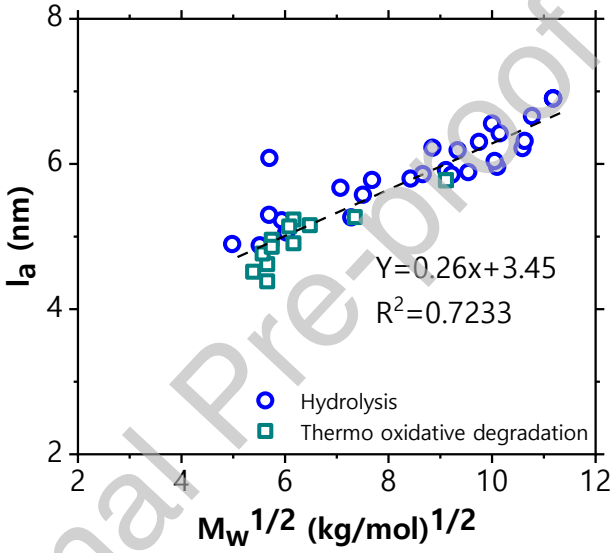


Figure 11 – Change in the amorphous layer thickness as a function of the square root of weight average molecular weight in polyamide 6

This equation is verified here for the first time for polyamide PA6; moreover, it is possible to directly link the amorphous thickness layer to $M_w$ with a value of $l_{ao}$ equal to 3.45 nm and α equal to 0.26 $(mol/kg)^{1/2}$. One interesting point is that this relationship can be applied even if the crystallinity ratio changes during ageing. As the polydispersity index (IP) is constant during ageing, it implies that $M_w$ and $M_n$ are proportional and so $l_a$ is directly related to the $M_n$ value. We can also link the ultimate tensile properties to the amorphous layer thickness (see Figure 12) with the same conclusions as for $M_n$. To sum up:

- An empirical relationship exists between maximal strain at break and $l_a$ for all the samples considered in this study;
- A critical amorphous layer thickness has been identified and is equal to 5 nm.

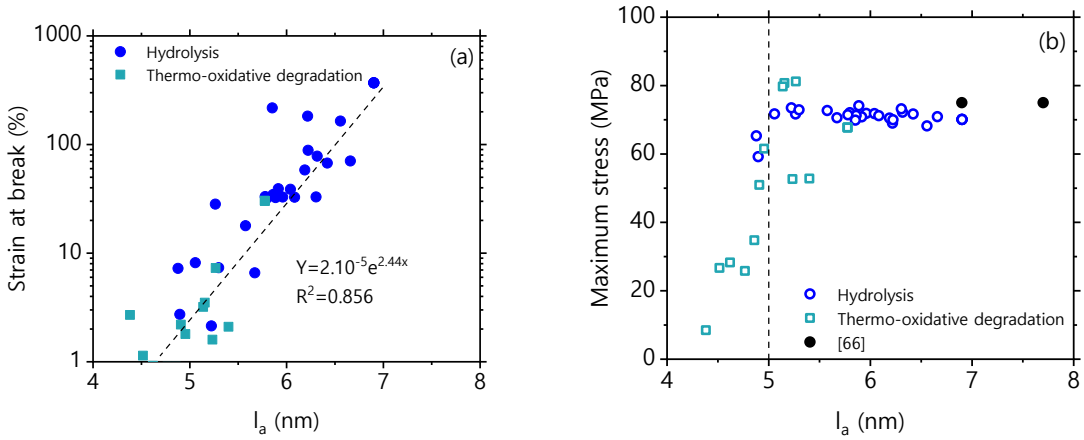


Figure 12 – Strain at break (a) and Maximal stress (b) as function of $l_a$ for all ageing conditions considered in this study and data availbale in litterature

As a conclusion, it clearly appears that both the molecular mass and the amorphous layer thickness can be used to describe embrittlement in polyamide. On the contrary, the crystallinity ratio is not an appropriate indicator to characterize embrittlement in this material.

## 4.2. Origin of the embrittlement in polyamide

### 4.2.1. Role of tie molecules in the decrease in strain at break

The mechanical properties of semi-crystalline polymers depend on the cohesive energy of the polymer but also on the ability of the polymer to transfer stresses between phases. The transmission of stresses is ensured by the so-called tie molecules which connect the amorphous phase and the crystalline phase. During chemical degradation, chain scission occurs randomly within the amorphous phase and can therefore affect these tie molecules. The experimental quantification of tie molecules cannot be directly determined, the estimation is quite complex. A theoretical approach is therefore preferred here. One first question is raised. Can the tie molecules exist for all the samples considered here? For a chain to be a tie molecule, its gyration radius ($R_g$) must be greater than the amorphous layer thickness ($l_a$), i.e. $l_a > R_g$ [59]. The radius of gyration represents the distance between each end of a chain and can be calculated from Equation 6 (Figure 13). We can observe that for all the samples considered here, $R_g$ is much larger than $L_a$ meaning that, in theory, tie molecules can exist.

$$R_g^2 = a^2 * M \quad \text{(Eq 6)}$$

Where $R_g$ is the radius of gyration, $a^2$ is the Kuhn length and equal to 8,53 nm².mol/kg for PA6 [60], and M the molar mass of the polymer

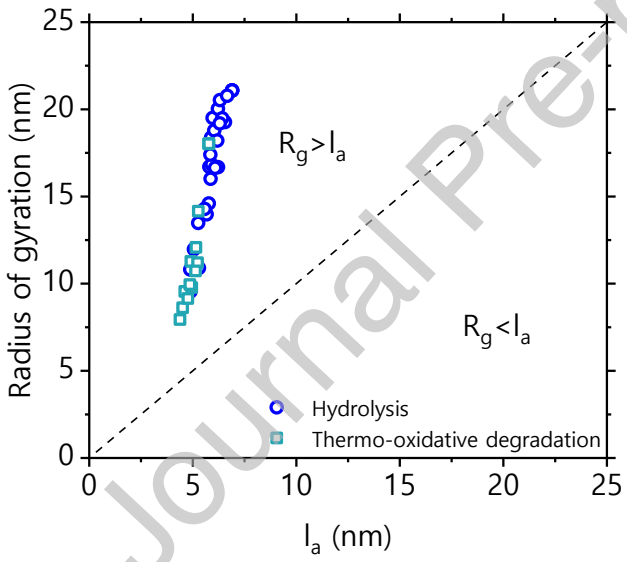


Figure 13 – Gyration radius calculated from Equation 6 as a function of amorphous layer thickness

Now that the potential existence of tie molecules has been demonstrated, let us focus on the probability of appearance of such molecules using theoretical considerations. This probability has been defined by Huang and Brown [61] and improved by Seguela [62], and can be calculated using the following equation (Equation 7):

$$P = \frac{1}{3}.\frac{\int_L^\infty r^2.exp(-\frac{3}{2}.\frac{r^2}{R_g^2}).dr}{\int_0^\infty r^2.exp(-\frac{3}{2}.\frac{r^2}{R_g^2}).dr} \quad \text{(Eq. 7)}$$

Where P is the probability of a molecule to be a tie molecule, $R_g$ the radius of gyration (nm) and L is given by the Equation 8:

$$L = 2l_c + l_a \quad \text{(Eq. 8)}$$

Where $l_c$ and $l_a$ are respectively the thickness of crystalline and amorphous layer (nm).

The probability of one molecule to be a tie molecule for PA6 hydrolysed at 100°C, has been plotted as a function of the molar mass in Figure 14. In the unaged sample, the probability of the presence of tie molecules is about 0.15. This decreases for ageing up to 250 days. For longer durations, the computed probability is close to 0. Those results have been compared to the strain at break and the maximum stress in Figure 14.a and Figure 14.b respectively. Two major points are highlighted here, first the decrease in strain at break occurs at the same time as the decrease in tie molecules probability. Second, in spite of the very small number of tie molecules, the maximal stress remains unchanged.

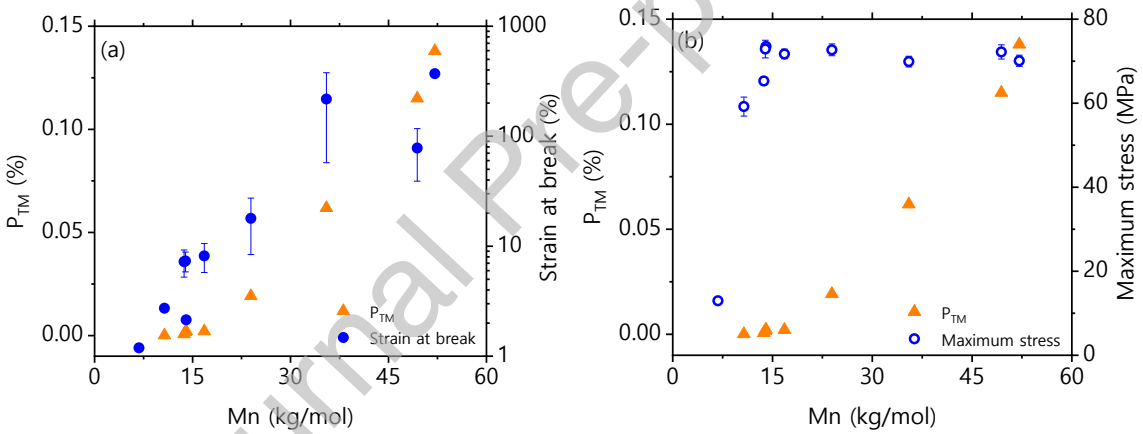


Figure 14 – Probability of tie molecule ($P_{TM}$) as a function of $M_n$ during ageing in water at 100°C compared with strain at break value (a) and maximal stress (b)

In order to explain the decrease in strain at break during chain scissions within polyamide, this value is plotted as a function of tie molecules probability for all the samples considered in this study in Figure 15. Even if there is some scattering due to the difficulty in the measurement of strain at break for aged films, a general trend is observed between the tie molecule probability and the maximal strain that can be applied to a PA6 before breakage. As the number of tie molecules decreases, the strain at break drops. This means that during chemical degradation that involves chain scissions, the decrease in elongation at break can be explained by the reduction of tie molecules concentration. For the maximum stress no correlation has been observed.

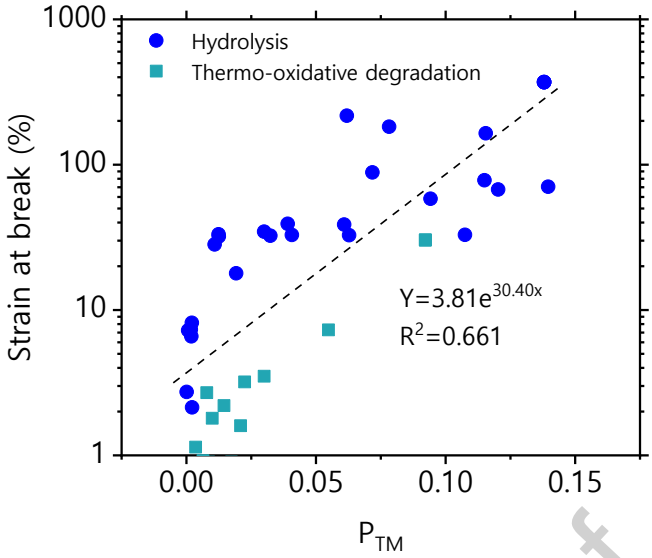


Figure 15 – Strain at break as a function of tie molecule probability ($P_{TM}$)

### 4.2.2. Entanglement to explain the drop in maximal stress

During the chain scission process the maximal stress remains unchanged as long as the molecular mass is above a critical value (here 15 kg/mol) and the amorphous layer thickness above 5 nm. Then when these values are reached a drop in maximal stress occurs. It is worth noting that we have shown that the maximal stress is not affected by the decrease in tie molecules. So we will focus on entanglements in order to explain this behaviour. To do so, the average number of entanglements per chain is calculated using Equation 9:

$$q = \frac{M_n}{M_e} \quad \text{(Eq. 9)}$$

Where q is the number of entanglements within the polymer, $M_n$ the molar mass of the polymer (kg/mol) and $M_e$ the molar mass between entanglements (equal to 2.2 kg/mol for PA6 [35]).

Figure 16 presents the maximal stress as a function of the number of entanglements within the polyamide for all samples from this study and also data from the literature [63–66]. A general behaviour can be identified: when the entanglement number is superior to 5 then the maximal stress is unchanged; on the contrary when the number of entanglements is inferior to 5 then the polyamide is brittle. These results clearly show that the drop in maximum stress is directly related to the entanglements number of the polymer. Moreover, this critical value is in accordance with previous published studies for semi crystalline polymers with an amorphous phase in the glassy state, for which the critical number of entanglements is equal to 5 [16,25].

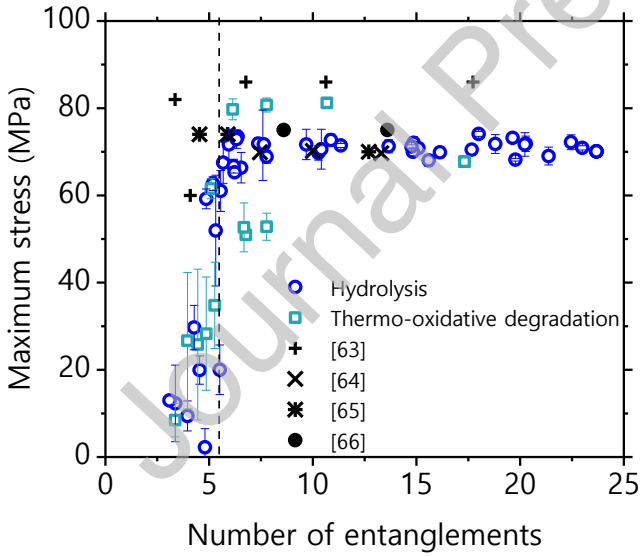


Figure 16: Maximum stress as a function of number of entanglements

To conclude on the origin of the embrittlement in PA during a chain scission process, first a decrease in the strain at break is observed whereas the maximum stress remains unchanged. This decrease in strain at break can be attributed to the decline in tie molecule concentration. This decrease is explained by the chain scission process that reduces the length of macromolecules. However, the drop off in maximum stress is not related to tie molecules but to the number of entanglements within the polymer. When the macromolecular length is not long enough to ensure a minimum of entanglements and that a stress is applied, then macromolecules can slide and so the polyamide exhibits a brittle behaviour.

## 5. Conclusion

Polyamide 6 samples were aged in both water without oxygen and air at several temperatures from 80°C to 140°C, with a maximal ageing duration of 24 months. Then both the polymer structure and the mechanical properties were characterized. In the two cases (i.e. oxidation and hydrolysis), the degradation process leads to chain scissions in the amorphous phase of PA6 and induces an increase in the macromolecular mobility and then a chemi-crystallization phenomenon. The latter results in a growth of crystallinity ratio. The tensile behaviour is also largely affected by these degradations. First a decrease in strain at break is observed while the maximal stress remains unchanged. Then, for high degradation levels a drop off in maximal stress occurs.

Using these experimental results, relationships between the polymer structure and its mechanical behaviour were considered. The objective was to understand the origin of the embrittlement in polyamide as well as establishing the factors governing the change in mechanical behaviour.

The decrease in strain at break during chemical degradation is attributed to the decrease in tie molecules within the polymer. During a chain scission process, tie molecules are cut off and decrease in number with ageing. It results that the stress transfer from amorphous layer to crystalline layer is no longer maintained. However, even if the number of tie molecules is very low, the stress at break remains unchanged. For extended degradation, a drop in maximal stress finally occurs. It has been demonstrated that this is related to the lack of entanglements within the polymer, which allows the macromolecules to slip when loading is applied.

From a practical point of view, it appears that crystallinity ratio cannot be used to describe embrittlement in polyamide. However, both the molar mass and the amorphous layer thickness are structural parameters that can be used to describe faithfully the mechanical behaviour changes during chemical degradation processes.

# Sample CRediT author statement

Q.Deshoulles M.Le Gall C.Dreanno M.Arhant G Stoclet D.Priour P -Y.Le Gac

Conceptualization, Methodology, Data curation, Writing, Reviewing and Editing

## Acknowledgement

The authors would like to thank the Merlin Microplastics project funded by Ifremer. Financial support from Région Nord Pas-de-Calais and European FEDER for the SAXS laboratory equipment is gratefully acknowledged. Quentin Deshoulles was supported by a Région Bretagne fellowship. We gratefully acknowledge the contributions of Christophe Peyronnet and Mickael Premel Cabic (Ifremer) for their technical assistance and advice.

References

[1] J.P.G.L. Frias, R. Nash, Microplastics: Finding a consensus on the definition, Mar. Pollut. Bull. 138 (2019) 145–147. https://doi.org/10.1016/j.marpolbul.2018.11.022.

[2] A. ter Halle, L. Ladirat, X. Gendre, D. Goudouneche, C. Pusineri, C. Routaboul, C. Tenailleau, .B Duployer, E. Perez, Understanding the Fragmentation Pattern of Marine Plastic Debris, Environ. Sci. Technol. 50 (2016) 5668–5675. https://doi.org/10.1021/acs.est.6b00594.

[3] A.L. Andrady, The plastic in microplastics: A review, Mar. Pollut. Bull. 119 (2017) 12–22. https://doi.org/10.1016/j.marpolbul.2017.01.082.

[4] E. Mofakhami, S. Tencé-Girault, J. Perrin, M. Scheel, L. Gervat, C. Ovalle, L. Laiarinandrasana, B. Fayolle, G. Miquelard-Garnier, Microstructure-mechanical properties relationships in vibration welded glass-fiber-reinforced polyamide 66: A high-resolution X-ray microtomography study, Polym. Test. 85 (2020) 106454. https://doi.org/10.1016/j.polymertesting.2020.106454.

[5] M. Shirinbayan, A. Montazeri, M. Nouri Sedeh, N. Abbasnezhad, J. Fitoussi, A. Tcharkhrtchi, Rotational Molding of Polyamide-12 Nanocomposites: Modeling of the Viscoelastic Behavior, Int. J. Mater. Form. 14 (2021) 143–152. https://doi.org/10.1007/s12289-020-01558-9.

[6] M. Broudin, V. Le Saux, P.-Y. Le Gac, C. Champy, G. Robert, P. Charrier, Y. Marco, Moisture sorption in polyamide 6.6: Experimental investigation and comparison to four physical-based models, Polym. Test. 43 (2015) 10–20. https://doi.org/10.1016/j.polymertesting.2015.02.004.

[7] C. Humeau, P. Davies, P.-Y. LeGac, F. Jacquemin, Influence of water on the short and long term mechanical behaviour of polyamide 6 (nylon) fibres and yarns, Multiscale Multidiscip. Model. Exp. Des. 1 (2018) 317–327. https://doi.org/10.1007/s41939-018-0036-6.

[8] J. Wesołowski, K. Płachta, The Polyamide Market, Fibres Text. East. Eur. Nr 6 (120) (2016). https://doi.org/10.5604/12303666.1215537.

[9] M. Arhant, P.-Y. Le Gac, M. Le Gall, C. Burtin, C. Briançon, P. Davies, Modelling the non Fickian water absorption in polyamide 6, Polym. Degrad. Stab. 133 (2016) 404–412. https://doi.org/10.1016/j.polymdegradstab.2016.09.001.

[10] H.K. Reimschuessel, Relationships on the effect of water on glass transition temperature and young's modulus of nylon 6, J. Polym. Sci. Polym. Chem. Ed. 16 (1978) 1229–1236. https://doi.org/10.1002/pol.1978.170160606.

[11] P.-Y. Le Gac, M. Arhant, M. Le Gall, P. Davies, Yield stress changes induced by water in polyamide 6: Characterization and modeling, Polym. Degrad. Stab. 137 (2017) 272–280. https://doi.org/10.1016/j.polymdegradstab.2017.02.003.

[12] E. Richaud, O. Okamba Diogo, B. Fayolle, J. Verdu, J. Guilment, F. Fernagut, Review: Auto-oxidation of aliphatic polyamides, Polym. Degrad. Stab. 98 (2013) 1929–1939. https://doi.org/10.1016/j.polymdegradstab.2013.04.012.

[13] R. Bernstein, D.K. Derzon, K.T. Gillen, Nylon 6.6 accelerated aging studies: thermal–oxidative degradation and its interaction with hydrolysis, Polym. Degrad. Stab. 88 (2005) 480–488. https://doi.org/10.1016/j.polymdegradstab.2004.11.020.

[14] B. Jacques, M. Werth, I. Merdas, F. Thominette, J. Verdu, Hydrolytic ageing of polyamide 11. 1. Hydrolysis kinetics in water, Polymer. 43 (2002) 6439–6447. https://doi.org/10.1016/S0032-3861(02)00583-9.

[15] O. Okamba-Diogo, F. Fernagut, J. Guilment, F. Pery, B. Fayolle, E. Richaud, Thermal stabilization of polyamide 11 by phenolic antioxidants, Polym. Degrad. Stab. 179 (2020) 109206. https://doi.org/10.1016/j.polymdegradstab.2020.109206.

[16] O. Okamba-Diogo, E. Richaud, J. Verdu, F. Fernagut, J. Guilment, B. Fayolle, Investigation of polyamide 11 embrittlement during oxidative degradation, Polymer. 82 (2016) 49–56. https://doi.org/10.1016/j.polymer.2015.11.025.

[17] P.-Y. Le Gac, B. Fayolle, Impact of fillers (short glass fibers and rubber) on the hydrolysis-induced embrittlement of polyamide 6.6, Compos. Part B Eng. 153 (2018) 256–263. https://doi.org/10.1016/j.compositesb.2018.07.028.

[18] B. Fayolle, E. Richaud, X. Colin, J. Verdu, Review: degradation-induced embrittlement in semi-crystalline polymers having their amorphous phase in rubbery state, J. Mater. Sci. 43 (2008) 6999–7012. https://doi.org/10.1007/s10853-008-3005-3.

[19] B. Fayolle, L. Audouin, J. Verdu, A critical molar mass separating the ductile and brittle regimes as revealed by thermal oxidation in polypropylene, Polymer. 45 (2004) 4323–4330. https://doi.org/10.1016/j.polymer.2004.03.069.

[20] C. Creton, E.J. Kramer, H.R. Brown, C.-Y. Hui, Adhesion and Fracture of Interfaces Between Immiscible Polymers: from the Molecular to the Continuum Scal, in: Mol. Simul. Fract. Gel Theory, Springer Berlin Heidelberg, Berlin, Heidelberg, 2002: pp. 53–136. https://doi.org/10.1007/3-540-45141-2_2.

[21] B. Fayolle, L. Audouin, J. Verdu, Oxidation induced embrittlement in polypropylene Ð a tensile testing study, Polym. Degrad. Stab. (2000) 8.

[22] A.F. Reano, A. Guinault, E. Richaud, B. Fayolle, Polyethylene loss of ductility during oxidation: Effect of initial molar mass distribution, Polym. Degrad. Stab. 149 (2018) 78–84. https://doi.org/10.1016/j.polymdegradstab.2018.01.021.

[23] S.J.A. Hocker, W.T. Kim, H.C. Schniepp, D.E. Kranbuehl, Polymer crystallinity and the ductile to brittle transition, Polymer. 158 (2018) 72–76. https://doi.org/10.1016/j.polymer.2018.10.031.

[24] F. Julienne, F. Lagarde, N. Delorme, Influence of the crystalline structure on the fragmentation of weathered polyolefines, Polym. Degrad. Stab. 170 (2019) 109012. https://doi.org/10.1016/j.polymdegradstab.2019.109012.

[25] M. Arhant, M. Le Gall, P.-Y. Le Gac, P. Davies, Impact of hydrolytic degradation on mechanical properties of PET - Towards an understanding of microplastics formation, Polym. Degrad. Stab. 161 (2019) 175–182. https://doi.org/10.1016/j.polymdegradstab.2019.01.021.

[26] B. Fayolle, X. Colin, L. Audouin, J. Verdu, Mechanism of degradation induced embrittlement in polyethylene, Polym. Degrad. Stab. 92 (2007) 231–238. https://doi.org/10.1016/j.polymdegradstab.2006.11.012.

[27] Y.-C. Hsu, M.P. Weir, R.W. Truss, C.J. Garvey, T.M. Nicholson, P.J. Halley, A fundamental study on photo-oxidative degradation of linear low density polyethylene films at embrittlement, Polymer. 53 (2012) 2385–2393. https://doi.org/10.1016/j.polymer.2012.03.044.

[28] M.A. Kennedy, A.J. Peacock, L. Mandelkern, Tensile Properties of Crystalline Polymers: Linear Polyethylene, Macromolecules. 27 (1994) 5297–5310. https://doi.org/10.1021/ma00097a009.

[29] G.-F. Shan, W. Yang, M. Yang, B. Xie, J. Feng, Q. Fu, Effect of temperature and strain rate on the tensile deformation of polyamide 6, Polymer. 48 (2007) 2958–2968. https://doi.org/10.1016/j.polymer.2007.03.013.

[30] X.-F. Wei, K.J. Kallio, S. Bruder, M. Bellander, H.-H. Kausch, U.W. Gedde, M.S. Hedenqvist, Diffusion-limited oxidation of polyamide: Three stages of fracture behavior, Polym. Degrad. Stab. 154 (2018) 73–83. https://doi.org/10.1016/j.polymdegradstab.2018.05.024.

[31] P. Gijsman, W. Dong, A. Quintana, M. Celina, Influence of temperature and stabilization on oxygen diffusion limited oxidation profiles of polyamide 6, Polym. Degrad. Stab. 130 (2016) 83–96. https://doi.org/10.1016/j.polymdegradstab.2016.05.024.

[32] Q. Deshoulles, M. Le Gall, C. Dreanno, M. Arhant, D. Priour, P.-Y. Le Gac, Modelling pure polyamide 6 hydrolysis: Influence of water content in the amorphous phase, Polym. Degrad. Stab. 183 (2021) 109435. https://doi.org/10.1016/j.polymdegradstab.2020.109435.

[33] S. Laun, H. Pasch, N. Longiéras, C. Degoulet, Molar mass analysis of polyamides-11 and -12 by size exclusion chromatography in HFiP, Polymer. 49 (2008) 4502–4509. https://doi.org/10.1016/j.polymer.2008.08.017.

[34] K.-H. Illers, Polymorphie, kristallinität und schmelzwärme von poly(ε-caprolactam), 2. Kalorimetrische untersuchungen, Makromol. Chem. 179 (1978) 497–507. https://doi.org/10.1002/macp.1978.021790224.

[35] C. Millot, L.-A. Fillot, O. Lame, P. Sotta, R. Seguela, Assessment of polyamide-6 crystallinity by DSC, J. Therm. Anal. Calorim. 122 (2015) 307–314. https://doi.org/10.1007/s10973-015-4670-5.

[36] ISO 37:2017(en), Rubber, vulcanized or thermoplastic — Determination of tensile stress-strain properties, (n.d.). https://www.iso.org/obp/ui/#iso:std:iso:37:ed-6:v1:en (accessed April 23, 2021).

[37] S. Hocker, A.K. Rhudy, G. Ginsburg, D.E. Kranbuehl, Polyamide hydrolysis accelerated by small weak organic acids, Polymer. 55 (2014) 5057–5064. https://doi.org/10.1016/j.polymer.2014.08.010.

[38] N. Chaupart, G. Serpe, J. Verdu, Molecular weight distribution and mass changes during polyamide hydrolysis, Polymer. 39 (1998) 1375–1380. https://doi.org/10.1016/S0032-3861(97)00414-X.

[39] W. Dong, P. Gijsman, Influence of temperature on the thermo-oxidative degradation of polyamide 6 films, Polym. Degrad. Stab. 95 (2010) 1054–1062. https://doi.org/10.1016/j.polymdegradstab.2010.02.030.

[40] O. Okamba-Diogo, E. Richaud, J. Verdu, F. Fernagut, J. Guilment, B. Fayolle, Molecular and macromolecular structure changes in polyamide 11 during thermal oxidation,

Polym. Degrad. Stab. 108 (2014) 123–132. https://doi.org/10.1016/j.polymdegradstab.2014.05.028.

[41] G. Papet, L. Jirackova-Audouin, J. Verdu, Diffusion controlled radiochemical oxidation of low density polyethylene-I. Depth dependence of morphological changes, Radiat. Phys. Chem. 29 (1987) 65–69.

[42] K. Hoashi, R.D. Andrews, Morphological changes in nylon 6 and effect on mechanical properties. II. Dynamic mechanical properties, J. Polym. Sci. Part C Polym. Symp. 38 (1972) 387–404. https://doi.org/10.1002/polc.5070380131.

[43] J.P. Parker, P.H. Lindenmeyer, On the crystal structure of nylon 6, J. Appl. Polym. Sci. 21 (1977) 821–837. https://doi.org/10.1002/app.1977.070210322.

[44] G. Gurato, A. Fichera, F.Z. Grandi, R. Zannetti, P. Canal, Crystallinity and polymorphism of 6-polyamide, Makromol. Chem. 175 (1974) 953–975. https://doi.org/10.1002/macp.1974.021750322.

[45] N.S. Murthy, S.M. Aharoni, A.B. Szollosi, Stability of the γ form and the development of the α form in nylon 6, J. Polym. Sci. Polym. Phys. Ed. 23 (1985) 2549–2565. https://doi.org/10.1002/pol.1985.180231212.

[46] J. Gianchandani, J.E. Spruiell, E.S. Clark, Polymorphism and orientation development in melt spinning, drawing, and annealing of nylon-6 filaments, J. Appl. Polym. Sci. 27 (1982) 3527–3551. https://doi.org/10.1002/app.1982.070270928.

[47] A. Pawlak, A. Galeski, Plastic Deformation of Crystalline Polymers: The Role of Cavitation and Crystal Plasticity, Macromolecules. 38 (2005) 9688–9697. https://doi.org/10.1021/ma050842o.

[48] M. Deroiné, A. Le Duigou, Y.-M. Corre, P.-Y. Le Gac, P. Davies, G. César, S. Bruzaud, Accelerated ageing and lifetime prediction of poly(3-hydroxybutyrate-co-3-hydroxyvalerate) in distilled water, Polym. Test. 39 (2014) 70–78. https://doi.org/10.1016/j.polymertesting.2014.07.018.

[49] R. Bernstein, K.T. Gillen, Nylon 6.6 accelerating aging studies: II. Long-term thermal-oxidative and hydrolysis results, Polym. Degrad. Stab. 95 (2010) 1471–1479. https://doi.org/10.1016/j.polymdegradstab.2010.06.018.

[50] K.T. Gillen, M. Celina, The wear-out approach for predicting the remaining lifetime of materials, Polym. Degrad. Stab. 71 (2000) 15–30. https://doi.org/10.1016/S0141-3910(00)00112-9.

[51] S. Maïza, X. Lefebvre, N. Brusselle-Dupend, M.-H. Klopffer, L. Cangémi, S. Castagnet, J.-C. Grandidier, Physicochemical and mechanical degradation of polyamide 11 induced by hydrolysis and thermal aging, J. Appl. Polym. Sci. 136 (2019) 47628. https://doi.org/10.1002/app.47628.

[52] C. El-Mazry, O. Correc, X. Colin, A new kinetic model for predicting polyamide 6-6 hydrolysis and its mechanical embrittlement, Polym. Degrad. Stab. 97 (2012) 1049–1059. https://doi.org/10.1016/j.polymdegradstab.2012.03.003.

[53] B. Fayolle, J. Verdu, Radiation aging and chemi-crystallization processes in polyoxymethylene, Eur. Polym. J. 47 (2011) 2145–2151. https://doi.org/10.1016/j.eurpolymj.2011.08.003.

[54] B. Fayolle, L. Audouin, J. Verdu, Radiation induced embrittlement of PTFE, Polymer. 44 (2003) 2773–2780. https://doi.org/10.1016/S0032-3861(03)00116-2.

[55] C. El-Mazry, M. Ben Hassine, O. Correc, X. Colin, Thermal oxidation kinetics of additive free polyamide 6-6, Polym. Degrad. Stab. 98 (2013) 22–36. https://doi.org/10.1016/j.polymdegradstab.2012.11.002.

[56] D. Forsström, B. Terselius, Thermo oxidative stability of polyamide 6 films I. Mechanical and chemical characterisation, Polym. Degrad. Stab. 67 (2000) 69–78. https://doi.org/10.1016/S0141-3910(99)00122-6.

[57] K. Majewski, S.C. Mantell, M. Bhattacharya, Relationship between morphological changes and mechanical properties in HDPE films exposed to a chlorinated environment, Polym. Degrad. Stab. 171 (2020) 109027. https://doi.org/10.1016/j.polymdegradstab.2019.109027.

[58] E. Robelin-Souffache, J. Rault, Origin of the long period and crystallinity in quenched semicrystalline polymers. 1, Macromolecules. 22 (1989) 3581–3594. https://doi.org/10.1021/ma00199a015.

[59] O. Darras, R. Séguéla, Crystallization-induced gelation of ethylene/1-butene copolymers over a wide crystallinity range, Colloid Polym. Sci. 273 (1995) 753–765. https://doi.org/10.1007/BF00658753.

[60] L.J. Fetters, D.J. Lohse, D. Richter, T.A. Witten, A. Zirkel, Connection between Polymer Molecular Weight, Density, Chain Dimensions, and Melt Viscoelastic Properties, Macromolecules. 27 (1994) 4639–4647. https://doi.org/10.1021/ma00095a001.

[61] Y.-L. Huang, N. Brown, Dependence of slow crack growth in polyethylene on butyl branch density: Morphology and theory, J. Polym. Sci. Part B Polym. Phys. 29 (1991) 129–137. https://doi.org/10.1002/polb.1991.090290116.

[62] R. Seguela, Critical review of the molecular topology of semicrystalline polymers: The origin and assessment of intercrystalline tie molecules and chain entanglements, J. Polym. Sci. Part B Polym. Phys. 43 (2005) 1729–1748. https://doi.org/10.1002/polb.20414.

[63] T.J. Bessell, D. Hull, J.B. Shortall, The effect of polymerization conditions and crystallinity on the mechanical properties and fracture of spherulitic nylon 6, J. Mater. Sci. 10 (1975) 1127–1136. https://doi.org/10.1007/BF00541393.

[64] T.D. Fornes, P.J. Yoon, H. Keskkula, D.R. Paul, Nylon 6 nanocomposites: the effect of matrix molecular weight, Polymer. 42 (2001) 09929–09940. https://doi.org/10.1016/S0032-3861(01)00552-3.

[65] P. Steeman, A. Nijenhuis, The effect of random branching on the balance between flow and mechanical properties of polyamide-6, Polymer. 51 (2010) 2700–2707. https://doi.org/10.1016/j.polymer.2010.04.017.

[66] C. Millot, R. Séguéla, O. Lame, L.-A. Fillot, C. Rochas, P. Sotta, Tensile Deformation of Bulk Polyamide 6 in the Preyield Strain Range. Micro–Macro Strain Relationships via in Situ SAXS and WAXS, Macromolecules. 50 (2017) 1541–1553. https://doi.org/10.1021/acs.macromol.6b02471.